

# Searching for LFV Flavon decays at hadron colliders

M. A. Arroyo-Ureña, J. L. Díaz-Cruz, and G. Tavares-Velasco,

Facultad de Ciencias Físico-Matemáticas, Benemérita Universidad Autónoma de Puebla, Puebla, México.

A. Bolaños

Departamento de Ciencias e Ingenierías, Universidad Iberoamericana, Campus Puebla, Puebla, México.

G. Hernández-Tomé

Departamento de Física, CINVESTAV IPN, Apartado Postal 14-740, 07000, México D. F., México.

(Dated: December 3, 2024)

The search for Flavons with a mass of  $\mathcal{O}(1)$  TeV at current and future colliders might probe low-scale flavor models. We are interested in the simplest model that invokes the Froggatt-Nielsen (FN) mechanism with an Abelian flavor symmetry, which includes a Higgs doublet and a FN complex singlet. Assuming a CP conserving scalar potential, there are a  $CP$ -even  $H_F$  and a  $CP$ -odd  $A_F$  Flavons with lepton flavor violating (LFV) couplings. The former can mix with the standard-model-like Higgs boson, thereby inducing tree-level LFV Higgs interactions that may be at the reach of the LHC. We study the constraints on the parameter space of the model from low-energy LFV processes, which are then used to evaluate the Flavon decay widths and the  $gg \rightarrow \phi \rightarrow \tau\mu$  ( $\phi = H_F, A_F$ ) production cross section at hadron colliders. After imposing several kinematic cuts to reduce the SM main background, we find that for  $m_{H_F}$  about 200–350 GeV, the decay  $H_F \rightarrow \tau\mu$  might be at the reach of the LHC for a luminosity in the range 1–3  $\text{ab}^{-1}$ , however, a luminosity of the order of 10  $\text{ab}^{-1}$  would be required to detect the  $A_F \rightarrow \tau\mu$  decay. On the other hand a future 100 TeV  $pp$  collider could probe masses as high as  $\mathcal{O}(10)$  TeV if it reaches an integrated luminosity of at least 20  $\text{ab}^{-1}$ . Therefore, the 100 TeV Collider could work as a Flavon factory.

PACS numbers:

## I. INTRODUCTION

After the discovery of a Higgs-like particle with a mass  $m_h = 125 - 126$  GeV [1, 2], the search for new physics (NP) has become the one of the next goals of the LHC. Although current measurements of the spin, parity, and couplings of the Higgs boson seem consistent with the standard model (SM) [3], its light mass seems troublesome, i.e. the hierarchy problem, and calls for new physics (NP). The SM has also other open issues, such as the flavor problem, unification, etc. [4, 5], which also encourages the study of NP models.

The couplings of the Higgs particle to a pair of massive gauge bosons or fermions have strengths proportional to the masses of such particles. However, the LHC has tested only a few of such Higgs couplings, namely the ones to the gauge bosons and the heaviest fermions. Along these lines, many studies have been devoted to analyze the pattern of Higgs couplings derived from LHC data, for instance [6, 7]. However, non-standard Higgs couplings, including the flavor violating (FV) ones, are predicted in many models of physics beyond the SM [8–11]. In particular, the observation of neutrino oscillations, which is associated with massive neutrinos, motivates the occurrence of lepton flavor violation (LFV) in nature [12]. Within the SM, LFV processes vanish at any order of perturbation theory, which motivates the study of SM extensions that predict sizeable LFV effects that could be at the reach of detection. Apart from decays such as  $l_i \rightarrow l_j \gamma$  and  $l_i \rightarrow l_j \bar{l}_k l_k$ , particularly interesting is the decay  $h \rightarrow \tau\mu$ , which was studied first in Refs. [13, 14], with subsequent analyses on the detectability of the signal appearing soon after [15, 16]. This motivated a plethora of calculations in the framework of several SM extensions, such as theories with massive neutrinos, supersymmetric theories, etc. [11, 17–22]. After the Higgs boson discovery, the decay  $h \rightarrow \tau\mu$  offers a great opportunity to search for NP at the LHC. Although a slight excess of the  $h \rightarrow \tau\mu$  branching ratio was reported at the LHC run I, with a significance of 2.4 standard deviations [23], a subsequent study [24] ruled out such an excess and put the limit  $BR(h \rightarrow \bar{\mu}\tau) < 1.2 \times 10^{-2}$  with 95% C.L. In the model we are interested in, LFV effects are induced at the tree-level in the scalar sector, so it is thus worth assessing their phenomenology.

Another open issue in the SM is the flavor problem [25], which has long been the focus of interest, with several proposals meant to address it, such as textures, GUT-inspired relations, symmetries, radiative generation, etc. In particular, a flavor symmetry approach can be supplemented with the Froggatt-Nielsen (FN) mechanism, which assumes that above some scale  $M_F$ , there is a symmetry (perhaps of Abelian type  $U(1)_F$ ) that forbids the appearance of Yukawa couplings; SM fermions are charged under this symmetry. However, the Yukawa matrices can arise through non-renormalizable operators. The Higgs spectrum of these models could include a light Flavon  $H_F$ , which could mix with the Higgs bosons when the flavor scale is of the order of the TeVs. Quite recently, the phenomenology of

Higgs-Flavons at particle colliders has been the focus of attention [26–30].

Although the states we are interested in arise from the mixing of Higgs bosons and Flavons, we will still call them Flavons for short. Depending on the particular model, there could be several potentially detectable Flavon decays, which would be indistinguishable from the decays of a heavy Higgs boson, therefore, to search for a distinctive signature, we will focus on the one arising from the LFV decay  $H_F \rightarrow \tau\mu$ , with  $\tau\mu = \tau^-\mu^+ + \tau^+\mu^-$ . The minimal model that introduces the FN mechanism with an Abelian flavor symmetry includes a scalar sector consisting of a Higgs doublet and a FN complex singlet. From now on we will refer to this model as the FN extension of the Standard Model (FNSM). Such a model predicts a  $CP$ -even Flavon  $H_F$  and a  $CP$ -odd one  $A_F$ . Also, the couplings of the light SM-like Higgs boson would deviate from the SM ones, such that two possible scenarios are possible: firstly, the mixing of the real part of the doublet with the real component of the FN singlet could induce sizable LFV Higgs couplings of the light physical Higgs boson, which might affect the light Higgs phenomenology; secondly, the  $CP$ -even Flavon could be very heavy, so its mixing with the light Higgs boson would be negligible and unconstrained by LHC Higgs data, though in such a case the  $CP$ -odd state  $A_F$  could be the lighter one, thereby giving rise to a potentially detectable LFV signal.

In this paper we are interested in studying the possible detection of both  $CP$ -even and  $CP$ -odd Flavons at the LHC and a future 100 TeV  $pp$  collider via their LFV decays. It has been pointed out that a 100 TeV  $pp$  collider would allow for a detailed study of several topics of interest in particle physics, such as Higgs physics and the electroweak symmetry breaking mechanism [31]. It will also be useful to search for possible signals of dark matter, SUSY theories, and other extension models [32].

We will start our analysis by considering the constraints on the parameter space of the FNSM obtained from Higgs data at the LHC, low energy LFV, and the muon magnetic dipole moment. A set of benchmarks will then be used to estimate the Flavon decay modes, focusing on the LFV ones, as well as their production cross sections by gluon fusion at the LHC and a future 100 TeV  $pp$  collider. We will then explore the possibility that the  $CP$ -even and  $CP$ -odd Flavons could be detected via the  $\tau\mu$  decay channel, for which we will make a Monte Carlo analysis of the signal and the SM main background.

The organization of our work is as follows. In Sec. II we describe the realization of the FN mechanism within the simplest model, namely that with one Higgs doublet and one FN singlet. In particular, we present the Higgs potential and Yukawa Lagrangian, from which the Flavon couplings can be extracted. Section III is devoted to the constraints on the parameters space of the model and the benchmarks of parameter values we will be using in our analysis, whereas Sec. IV is focused on the analysis of the decay modes of both a  $CP$ -even and a  $CP$ -odd Flavon as well as their production cross sections via gluon fusion at the LHC and a future 100 TeV  $pp$  collider. We also present the Monte Carlo analysis of the  $\mu\tau$  signal and its main background. The conclusions and outlook are presented in Sec. V.

## II. THE SCALAR SECTOR OF THE MINIMAL FNSM

The scalar sector of the FNSM includes the usual SM Higgs doublet

$$\Phi_1 = \begin{pmatrix} G^+ \\ \frac{1}{\sqrt{2}}(v + \phi^0 + iG_Z) \end{pmatrix}, \quad (1)$$

and a complex singlet

$$S_F = \frac{1}{\sqrt{2}}(u + s + ip), \quad (2)$$

where  $v$  denotes the SM vacuum expectation value (VEV) and  $u$  that of the FN singlet, whereas  $G^+$  and  $G^0$  will be identified with the pseudo-goldstone bosons that become the longitudinal modes of the  $W$  and  $Z$  gauge bosons.

### A. The Higgs potential

We turn now to discuss the minimal  $CP$ -conserving Higgs potential with a softly-broken  $U(1)$  global symmetry, which is given as follows

$$V = -\frac{1}{2}m_1^2\Phi_1^\dagger\Phi_1 - \frac{m_{s1}^2}{2}S_F^*S_F - \frac{m_{s2}^2}{2}(S_F^{*2} + S_F^2) + \frac{1}{2}\lambda_1(\Phi_1^\dagger\Phi_1)^2 + \lambda_s(S_F^*S_F)^2 + \lambda_{11}(\Phi_1^\dagger\Phi_1)(S_F^*S_F). \quad (3)$$

We are therefore left with the following  $U(1)$ -symmetric terms ( $m_1^2, m_{s1}^2, \lambda_1, \lambda_s, \lambda_{11}$ ), and the  $U(1)$ -soft-breaking term  $m_{s2}^2$ . The latter is required to avoid a massless Goldstone boson when  $\langle S \rangle = 0$ . An extensive analysis of this potential was presented in reference [33], where the parameter space that allows a viable model was identified.

Imposing the minimization conditions on  $V$  renders the following relations:

$$m_1^2 = v^2\lambda_1 + u^2\lambda_{11}, \quad (4)$$

$$m_{s1}^2 = -2m_{s2}^2 + 2u^2\lambda_s + v^2\lambda_{11}. \quad (5)$$

## B. The Scalar Mass Matrix

In a  $CP$ -invariant potential, the  $CP$ -even (real) and  $CP$ -odd (imaginary) components of the mass matrix do not mix. In this case the mass matrix for the real components in the basis  $(\phi^0, s)$  is given by:

$$M_S^2 = \begin{pmatrix} \lambda_1 v & \lambda_{11} u v \\ \lambda_{11} u v & 2\lambda_s u^2 \end{pmatrix}, \quad (6)$$

whereas the mass matrix for the imaginary components, in the basis  $(G_Z, p)$ , reads

$$M_P^2 = \begin{pmatrix} 0 & 0 \\ 0 & 2m_{s1}^2 \end{pmatrix}. \quad (7)$$

We notice that the mass scale for the  $CP$ -odd state arising from the FN singlet  $A_F = p$  is different from the VEV  $u$ , which is the  $U(1)$ -breaking scale, and therefore it could be much lighter. As for the mixing of the real components of the doublet  $\phi^0$  and the singlet  $s$ , the mass eigenstates are obtained through the standard  $2 \times 2$  rotation:

$$\phi^0 = \cos \alpha h + \sin \alpha H_F, \quad (8)$$

$$s = -\sin \alpha h + \cos \alpha H_F. \quad (9)$$

In what follows we will identify the mass eigenstate  $h$  as the SM-like Higgs boson with  $m_h = 125$  GeV, while the mass eigenstates  $H_F$  and  $A_F$  will be assumed to be heavier. Although they arise from Flavon-Higgs mixing, in the present work we will still refer to  $H_F$  and  $A_F$  as Flavons for short. The properties of the  $CP$ -even Flavon will depend on the size of its mixing with the lightest state. On the other hand, the  $CP$ -odd state, which does not couple to gauge bosons, it does couple to the SM fermions, including both diagonal and non-diagonal interactions.

Our analysis of Flavon decays requires the knowledge of cubic interactions, such as the trilinear vertex  $H_F h h$ , which is given in the minimal model by:

$$g_{H_F h h} = \frac{1}{2}[\lambda_{11}(u \cos^3 \alpha + v \sin^3 \alpha) + 2u \sin^2 \alpha \cos \alpha (3\lambda_s - \lambda_{11}) + v \sin \alpha \cos^2 \alpha (3\lambda_1 - 2\lambda_{11})]. \quad (10)$$

## C. Yukawa sector and LFV interactions

The FN Lagrangian of the model includes the terms that become the Yukawa couplings once the  $U(1)_F$  flavor symmetry is spontaneously broken. It is given by:

$$-\mathcal{L}_Y = \rho_{ij}^u \left( \frac{S_F}{\Lambda_F} \right)^{q_{ij}^u} \bar{Q}_i d_j \tilde{\Phi} + \rho_{ij}^d \left( \frac{S_F}{\Lambda_F} \right)^{q_{ij}^d} \bar{Q}_i u_j \Phi + \rho_{ij}^l \left( \frac{S_F}{\Lambda_F} \right)^{q_{ij}^l} \bar{L}_i l_j \Phi + \text{H.c.}, \quad (11)$$

where  $q_{ij}^f$  ( $f = u, d, l$ ) denote the Abelian charges that reproduce the observed fermion masses, for each fermion type. The Flavon field  $S_F$  is assumed to have flavor charge equal to -1, such that  $\mathcal{L}_Y$  is  $U(1)_F$ -invariant. Then, the Yukawa couplings arise after the spontaneous breaking of the flavor symmetry, i.e.  $\lambda_x = (\frac{S_F}{\Lambda_F})^{n_x}$ , where  $\langle S_F \rangle$  denotes the Flavon VEV, whereas  $\Lambda_F$  denotes a heavy mass scale, which represents the mass of heavy fields that transmit such symmetry breaking to the quarks and leptons. For specific examples of structures for the Yukawa matrices of fermion type, see [30].

In the unitary gauge we set  $G^\pm, G_Z \rightarrow 0$ , thus we can write the neutral component of the Higgs field as follows:

$$\Phi_0 = \frac{v + \phi_0}{\sqrt{2}}, \quad (12)$$

whereas the powers of the Flavon field can be expanded as

$$S^{q_{ij}^f} = \left( \frac{u + s + ip}{\sqrt{2}} \right)^{q_{ij}^f} \simeq \left( \frac{u}{\sqrt{2}} \right)^{q_{ij}^f} \left[ 1 + q_{ij}^f \left( \frac{s + ip}{u} \right) \right]. \quad (13)$$

Then, after substituting the Flavon mass eigenstates, one gets finally the following interaction Lagrangian for the Higgs-fermion couplings

$$\begin{aligned} -\mathcal{L}_Y = & \frac{1}{v} [\bar{U} \tilde{M}_u U + \bar{D} \tilde{M}_d D + \bar{L} \tilde{M}_l L] (c_\alpha h + s_\alpha H_F) \\ & + \frac{v}{\sqrt{2}u} [\bar{U}_i \tilde{Z}_{ij}^u U_j + \bar{D}_i \tilde{Z}_{ij}^d D_j + \bar{L}_i \tilde{Z}_{ij}^l L_j] (-s_\alpha h + c_\alpha H_F + iA_F) + \text{H.c.}, \end{aligned} \quad (14)$$

where we use the usual short-hand notation  $s_\alpha \equiv \sin \alpha$  and  $c_\alpha \equiv \cos \alpha$ . Here,  $\tilde{M}^f$  is the diagonal mixing matrix, whereas the information about the size of FV Higgs couplings is contained in the  $\tilde{Z}^f = U_L^f Z^f U_L^{f\dagger}$  matrices, with  $Z_{ij}^f$  given in the flavor basis as

$$Z_{ij}^f = \frac{v}{\sqrt{2}u} \rho_{ij}^f \left( \frac{u}{\sqrt{2}\Lambda_F} \right)^{q_{ij}^f} q_{ij}^f, \quad (15)$$

which remains non-diagonal once the fermion mass matrices are diagonalized, thereby giving rise to FV scalar couplings. The diagonal and non-diagonal interactions of the  $h$ ,  $H_F$ , and  $A_F$  scalar bosons with massive fermions are thus given by:

$$\begin{aligned} g_{hf_if_j} &= \frac{c_\alpha}{v} \tilde{M}_{ij}^f - s_\alpha r_s \tilde{Z}_{ij}^f, \\ g_{H_F f_i f_j} &= \frac{s_\alpha}{v} \tilde{M}_{ij}^f + c_\alpha r_s \tilde{Z}_{ij}^f, \\ g_{A_F f_i f_j} &= i r_s \tilde{Z}_{ij}^f, \end{aligned} \quad (16)$$

where the Feynman rule for the  $A_F f_i f_j$  vertex includes a  $\gamma^5$  Dirac matrix and  $r_s = v/(\sqrt{2}u)$ .

Besides the Yukawa couplings, we also need to specify the scalar-to-gauge-boson couplings. They can be readily extracted from the kinetic terms of the Higgs doublet and the singlet, which transforms trivially under the SM gauge group. Thus after substituting Eq. (8) in the kinetic term, we obtain that the  $h$  and  $H_F$  couplings to gauge boson pairs are SM-like, with the coupling constants given by  $g_{h_i VV} = \chi_V^{h_i} g_{h_{SM} VV}$  ( $V = W, Z$ ), for  $h_i = h, H_F$ , with  $\chi_V^h$  ( $\chi_V^{H_F}$ ) =  $\cos \alpha$  ( $\sin \alpha$ ). Thus the coupling constants are

$$g_{hZZ} = \frac{gm_Z}{c_W} \cos \alpha \quad (17)$$

$$g_{hWW} = gm_W \cos \alpha, \quad (18)$$

$$g_{H_F ZZ} = \frac{gm_Z}{c_W} \sin \alpha, \quad (19)$$

$$g_{H_F WW} = gm_W \sin \alpha. \quad (20)$$

We are interested in the possible detection of  $CP$ -even and  $CP$ -odd Flavons with masses of the TeV order at both the LHC and a future  $pp$  collider with a center-of-mass energy of 100 TeV. Depending on the particular model, there could be several potentially detectable decays of such Flavons, but some of them would also arise from heavy Higgs bosons, for instance within multi-Higgs doublet models. Thus, in order to search for a distinctive Flavon signature, we shall focus on the one arising from the LFV decay  $\phi \rightarrow \tau \mu$  ( $\phi = H_F, A_F$ ). In order to determine the detectability of this decay, we will present a Monte Carlo analysis of the signal and the most relevant SM backgrounds.

### III. CONSTRAINTS ON THE PARAMETER SPACE OF THE FNSM

In order to evaluate the Flavon decays and production modes at a hadron collider we need to analyze the most up-to-date constraints on the model parameters. For the mixing angle  $\alpha$  we can use the data obtained by the LHC collaborations on the Higgs boson properties, whereas the LFV couplings can be constrained via the experimental data on the muon anomalous magnetic dipole moment (AMDM)  $a_\mu$ , the LFV decays of the tau lepton  $\tau \rightarrow \bar{l}_i \bar{l}_j l_j$  and  $\tau \rightarrow l_i \gamma$ , as well as the experimental constraint on the  $h \rightarrow \mu\tau$  decay. All the necessary formulas to perform our analysis below are presented in Appendix A.

#### A. Mixing angle $\alpha$

We shall use the universal Higgs fit of Ref. [7], which presents constraints on the parameters  $\epsilon_X$ , defined as (small) deviations of the Higgs couplings from the SM values, i.e.  $\chi_X^h = g_{hXX}/g_{hXX}^{SM} = 1 + \epsilon_X$ . For the  $W$  and  $Z$  gauge bosons, the corresponding constraints are  $\epsilon_W = -0.15 \pm 0.14$  and  $\epsilon_Z = -0.01 \pm 0.13$ . Regarding the fermion couplings, we notice that this universal Higgs fit is valid for the  $CP$ -conserving case, which we are considering here; therefore we can apply them to constrain the properties of the  $CP$ -even SM-like Higgs boson. Furthermore, the constraints derived from the gauge interactions provide the strongest constraints on the mixing angle  $\alpha$ . Since the lightest scalar boson  $h$  couples with the SM gauge bosons with a strength that deviates from the SM couplings by the factor  $c_\alpha$ , to satisfy the bound on  $\epsilon_Z$  we need to have  $0.86 < c_\alpha < 1$ . We will use a conservative approach and use the benchmark  $c_\alpha = 0.95$  in our analysis below.

#### B. Diagonal $\tilde{Z}_{22}^l$ and $\tilde{Z}_{33}^l$ matrix elements

In this work we will use the 2-family approximation, neglecting FV with the leptons of the first fermion family. We will also assume that there is no  $CP$ -violating phase, which means that we have three free parameters:  $\tilde{Z}_{22}$ ,  $\tilde{Z}_{23}$ , and  $\tilde{Z}_{33}$ . To constrain the diagonal  $\tilde{Z}_{33}$  matrix element, we refer again to the universal Higgs fit of Ref. [7] and consider the constraint on the deviation of the SM  $h\bar{\tau}\tau$  coupling, namely,  $\epsilon_\tau = 0 \pm 0.18$ . We thus show in Fig. 1 the allowed area on the  $u - \tilde{Z}_{33}^l$  plane for two values of  $c_\alpha$ . We observe that in order to agree with the universal Higgs fit constraint when  $c_\alpha = 0.9$ ,  $\tilde{Z}_{33}^l$  must be of the order of  $10^{-3}$  for  $u = 0.5$  TeV and  $10^{-2}$  for  $u = 2$  TeV, but when  $c_\alpha = 0.95$  we must have values of the order  $10^{-2}$  in the complete  $u$  interval. Since we are considering  $c_\alpha = 0.95$ , we will use  $\tilde{Z}_{33}^l = 10^{-2}$  as benchmark.

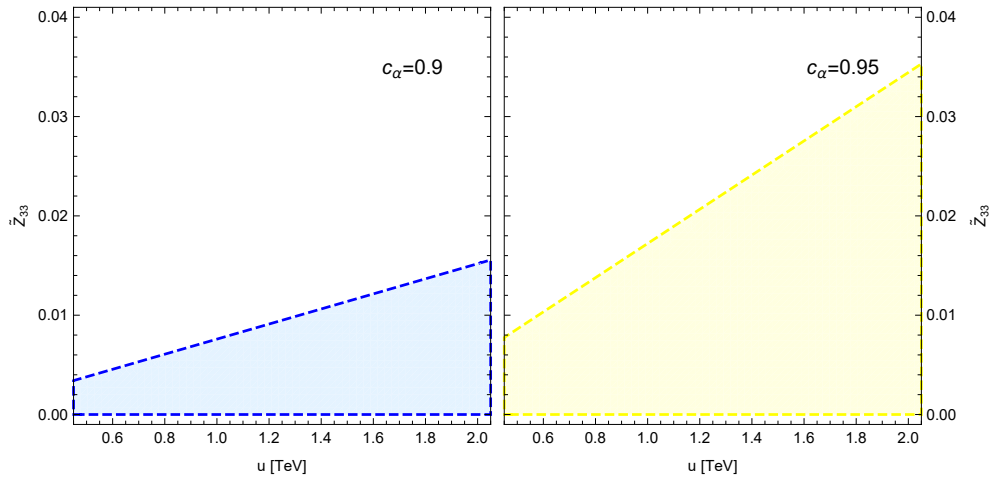


FIG. 1: Allowed area on the  $u - \tilde{Z}_{33}^l$  plane by the Higgs universal fit on  $\epsilon_\tau$  [7] for two values of  $c_\alpha$ .

As far as  $\tilde{Z}_{22}^l$  is concerned, there is no available data to constrain the  $h \rightarrow \bar{\mu}\mu$  coupling but we will assume the hierarchy  $\tilde{Z}_{22}^l < \tilde{Z}_{33}^l$  and set  $\tilde{Z}_{22}^l = 10^{-4}$ , otherwise the SM  $h \rightarrow \bar{\mu}\mu$  coupling would be swamped by the corrections of the FNSM.

### C. Non-diagonal $\tilde{Z}_{23}^l$ matrix element

We will consider the current experimental bounds on  $a_\mu$  [34], the tau decay  $\tau \rightarrow \mu\gamma$  [34], and the Higgs boson decay  $h \rightarrow \tau\mu$  [23, 35] to constrain the  $Z_{ij}^l$  matrix elements [36]. Notice that the current bound on the  $\tau \rightarrow 3\mu$  decay width gives very weak constraints, so we will omit such a process in our analysis. Two scenarios arise when dealing with constraints on LFV couplings:

- Scenario I: the FNSM is assumed to be responsible for the discrepancy between the theoretical and experimental values of the muon AMDM.
- Scenario II: the FNSM Flavons would not be responsible for the  $a_\mu$  discrepancy. It could happen instead that future calculations of the SM hadronic contribution would settle such a discrepancy without requiring any NP. Otherwise, the ultraviolet completion of the FNSM could give extra contributions, which would solve the  $a_\mu$  puzzle. In any case, by requiring that the new contribution from the Flavons to  $\Delta a_\mu$  is smaller than the experimental central value. We find that it is enough to satisfy the LHC constrain from  $h \rightarrow \tau\mu$  in order to have a viable parameter space.

We will now assess the implications of both scenarios. To avoid large corrections to the diagonal lepton scalar couplings, we will take  $\tilde{Z}_{22} \simeq 10^{-3}$  and  $\tilde{Z}_{33} \simeq 10^{-2}$ . We show in Fig. 2 the area allowed in the  $u - \tilde{Z}_{23}$  plane by the experimental constraints on the muon AMDM along with the  $\tau \rightarrow \mu\gamma$  and  $h \rightarrow \tau\mu$  decays for the indicated values of the Higgs Flavon masses and the mixing angle  $c_\alpha$ . We observe that scenario I is not consistent with the constraint on the  $\tilde{Z}_{23}$  matrix element from the  $h \rightarrow \mu\tau$  decay, which requires small values of this parameter, of the order of  $10^{-2}$  for  $u = 0.5$  TeV and  $10^{-1}$  for  $u = 2$  TeV, whereas the muon AMDM requires values of  $\tilde{Z}_{23}$  as large as 1 for  $u = 1$  TeV. Therefore we will assume scenario II and take as benchmark  $Z_{23} \simeq 0.1$ , which is allowed for  $u \simeq 1.5$  TeV.

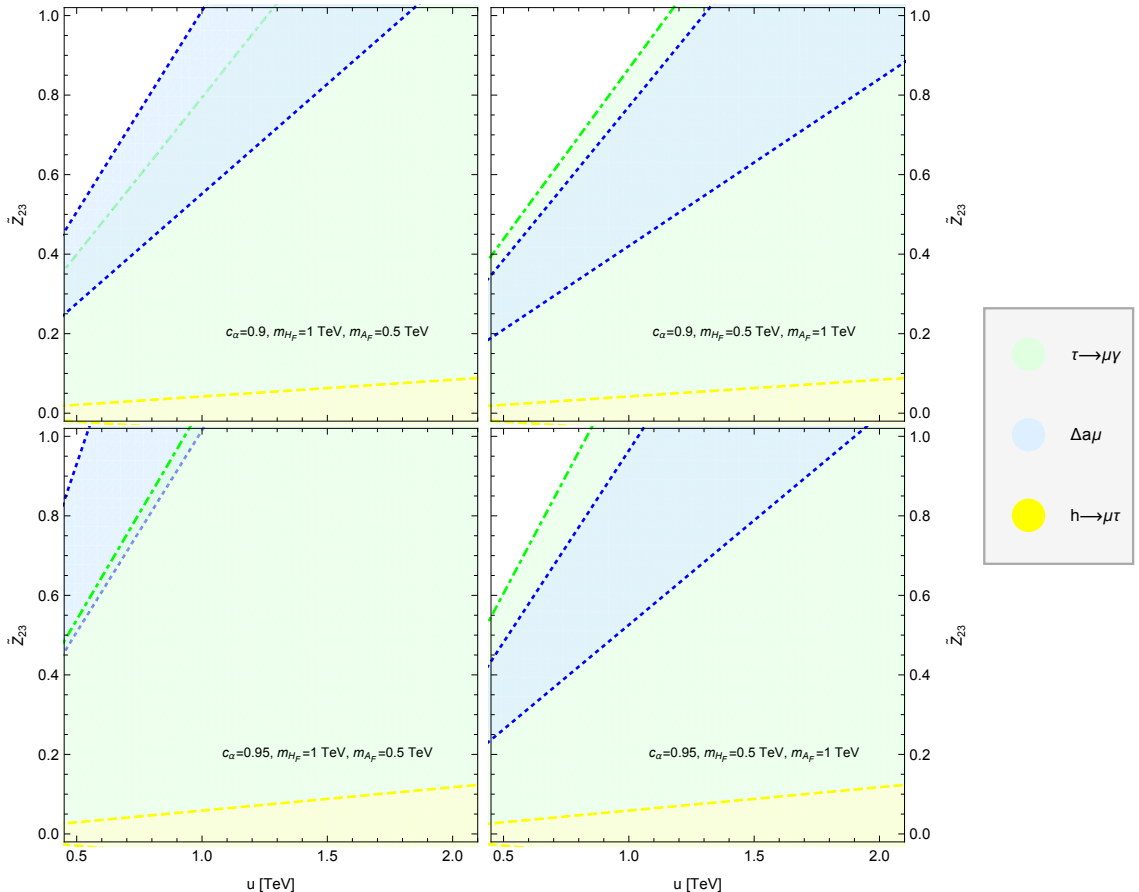


FIG. 2: Allowed area on the  $u - \tilde{Z}_{23}^l$  plane by the current experimental bounds on the muon AMDM, the  $\tau \rightarrow \mu\gamma$  decay, and the  $h \rightarrow \tau\mu$  decay for the indicated values of the model parameters.

TABLE I: Benchmarks used for the analysis of the production and detection of the Flavons  $H_F$  and  $A_F$  at the LHC and a future 100 TeV  $pp$  collider in the context of the FNSM.

Parameter	Benchmark
$c_\alpha$	0.95
$u$	1.5 TeV
$\tilde{Z}_{22}^l$	$10^{-4}$
$\tilde{Z}_{33}^l$	$10^{-2}$
$\tilde{Z}_{23}^l$	$10^{-1}$
$\lambda_{H_F hh}$	$0.1u$

#### D. $\tilde{Z}_{33}^u$ and $\tilde{Z}_{23}^u$ matrix elements

According to the universal Higgs fit [7], the allowed value for the deviation of the SM  $h\bar{t}$  coupling is  $\epsilon_t = -0.21 \pm 0.22$ . We will use again the two-family approximation and take the values  $\tilde{Z}_{33}^u = 0.01$  and  $\tilde{Z}_{23}^u = 0.1$ .

#### E. Summary of Benchmarks for the model parameters

In summary, in our study below we will use the following benchmarks:

1. Mixing angle  $\alpha$ : As discussed above, to satisfy the fit on the 125 GeV Higgs couplings measured at the LHC, the following constraint must be obeyed  $0.86 < c_\alpha < 1$ . We will thus use the benchmark  $c_\alpha = 0.95$ .
2. FN singlet VEV  $u$ : It appears in the Flavon couplings and the LFV SM Higgs coupling. We will consider the value 1.5 TeV.
3.  $\tilde{Z}_{ij}^f$  matrix: It determines the strength of the LFV scalar couplings. We will use the 2-family approximation and take  $\tilde{Z}_{22}^l = 10^{-4}$ ,  $\tilde{Z}_{33}^l = 10^{-2}$ , and  $\tilde{Z}_{23}^l = 10^{-1}$ , which are consistent with the constraint on the LFV decay  $h \rightarrow \mu\tau$ .
4.  $H_F hh$  interaction: This vertex depends on a combination of parameters that appear in the Higgs potential. However, these parameters could be traded by an effective coupling  $\lambda_{H_F hh}$ , which can take values of the order of  $O(1)$ . We will thus fix  $\lambda_{H_F hh} \simeq 0.1u$ .

A summary of the benchmarks we are going to consider in our analysis is presented in Table I.

## IV. SEARCH FOR LFV FLAVON DECAYS AT HADRON COLLIDERS

As stated above, the aim of this work is to analyze the detectability of the LFV signal arising from the Flavon decays, as predicted by the FNSM, at the LHC and a future 100 TeV  $pp$  collider. Below we will present an analysis concentrating on the main Flavon production mechanism, i.e. gluon fusion, as well as the branching ratios of its dominant decay modes. Then, we will present the Monte Carlo analysis of the  $H_F \rightarrow \tau\mu$  and  $A_F \rightarrow \tau\mu$  decay signatures, including the study of the potential SM background. We will present a conservative analysis meant to find out whether it is possible to have evidence of our signal at the LHC and the future 100 TeV  $pp$  collider.

#### A. Production cross-sections of the $CP$ -even and $CP$ -odd Flavons

We now turn to analyze the main production mode of both  $H_F$  and  $A_F$  Flavons at hadronic colliders, namely, by gluon fusion. The High-Luminosity Large Hadron Collider project aims to increase potential discoveries contemplating a luminosity of up to  $\mathcal{L}=3 \text{ ab}^{-1}$  about 2025. As far as a 100 TeV  $pp$  collider is concerned the future circular collider (FCC) contemplates an integrated luminosity of until  $\mathcal{O}(10 \text{ ab}^{-1})$ . We consider the integrated luminosities shown in the table II.

In Fig. 3 we show the  $pp \rightarrow H_F X$  production cross section of a  $CP$ -even Flavon as a function of its mass  $m_{H_F}$  at the LHC and a future 100 TeV  $pp$  collider. We also show the event numbers on the right axis of each plot. As far as the  $CP$ -odd Flavon is concerned, the respective production cross section and event numbers are presented in Fig. 4.

TABLE II: Integrated luminosities considered in our analysis.

Collider	Luminosity
HL-LHC	$0.3\text{-}3 \text{ ab}^{-1}$
FCC	$3\text{-}20 \text{ ab}^{-1}$

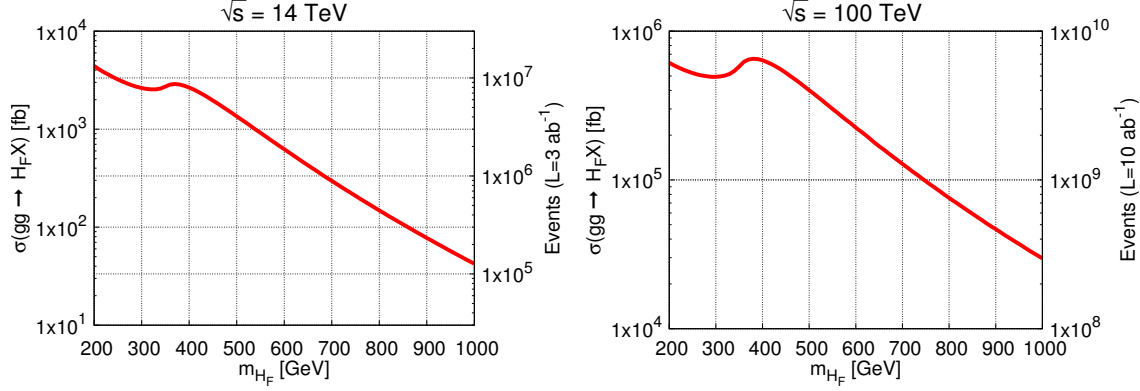


FIG. 3: Production cross-section  $\sigma(pp \rightarrow H_F X)$  of a  $CP$ -even Flavon at a hadronic collider as a function of its mass  $m_{H_F}$  for  $\sqrt{s} = 14$  (100) TeV. The event numbers obtained with an integrated luminosity of  $\mathcal{L} = 3$  (10)  $\text{ab}^{-1}$  are presented on the right axis.

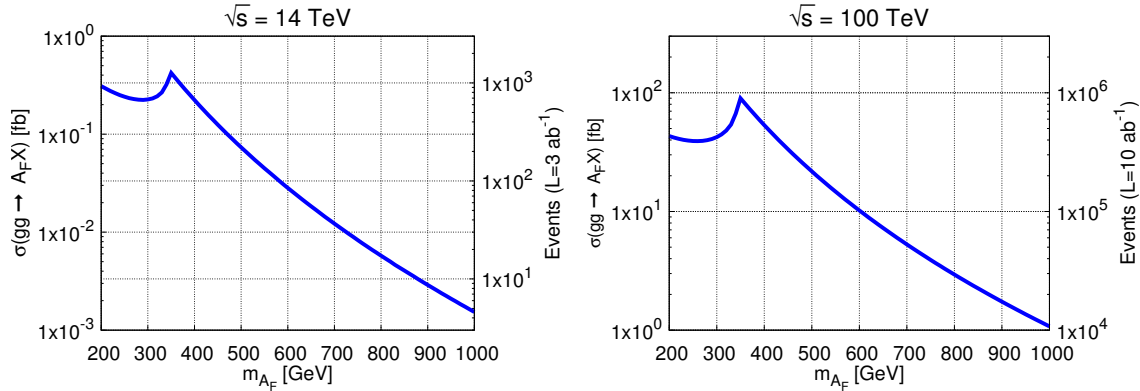


FIG. 4: The same as in Fig. 3 but for a  $CP$ -odd Flavon .

The dominant contribution to gluon fusion arises from loops carrying the top quark as shown in Fig 5. This explains the suppression of the production of the  $CP$ -odd Flavon as compared to that of the  $CP$ -even one, as observed in Figs. 3 and 4, which stems from the appearance of the coupling  $g_{A_F \bar{t}t}$  in the corresponding cross section. For instance, taking into account the parameter values of Table I, we have  $g_{A_F \bar{t}t}^2 \sim 10^{-6}$ , whereas for the  $CP$ -even Flavon  $g_{H_F \bar{t}t}^2 \sim 10^{-2}$ .

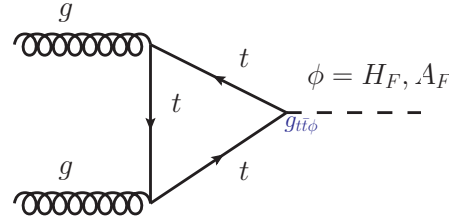


FIG. 5: Feynman diagram for the dominant contribution to Flavon production via gluon fusion at the leading order.

## B. Flavon decays

### 1. Two-body decays

We now analyze the behavior of the branching ratios of the dominant decay modes, including the FV ones, of both the  $CP$ -even and  $CP$ -odd Flavons. Analytical expressions for the partial decay widths are presented in Appendix B. It is worth mentioning that a crosscheck was done by comparing the numerical results obtained via our own C language code implementing the analytic expressions of Appendix B, and those computed with the aid of the CalcHEP package [37], for which we used an implementation of the FNSM Feynman rules obtained with LanHEP [38]. In Fig. 6 we present the relevant branching ratios of the decays modes of a  $CP$ -even Flavon as functions of its mass for the benchmarks of Table I.

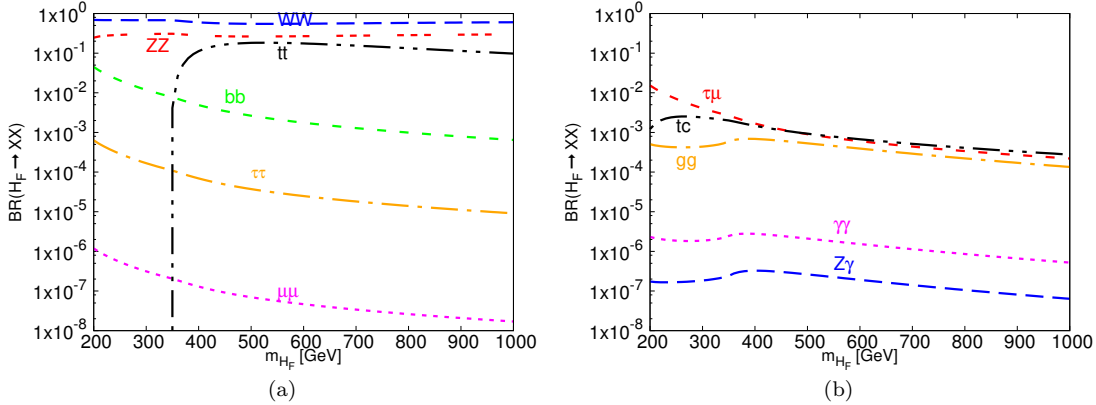


FIG. 6: Branching ratios of the two-body decay modes of a  $CP$ -even Flavon as a function of its mass for the parameter values of Table I.

We observe in Fig. 6 that in the scenario under study and for  $m_{H_F}$  ranging between 200 and 1000 GeV, the dominant  $H_F$  decay mode would be  $H_F \rightarrow WW$ , followed by  $H_F \rightarrow ZZ$ . Once the  $H_F \rightarrow \bar{t}t$  channel became open, its branching ratio would be about the same order of magnitude as that of the  $H_F \rightarrow ZZ$  decay. Other relevant decay modes would be  $H_F \rightarrow \bar{t}c$ ,  $H_F \rightarrow \bar{b}b$ , and  $H_F \rightarrow \tau\mu$ , whereas the one-loop induced decays  $H_F \rightarrow \gamma\gamma$  and  $H_F \rightarrow \gamma Z$  would have tiny branching ratios.

As far as the  $CP$ -odd Flavon  $A_F$  is concerned, since it does not couple to gauge bosons at the tree-level, its main decay modes are into fermion pairs. The corresponding branching ratios are shown in Fig. 7. We observe that the decay modes  $A_F \rightarrow \bar{f}f$  could have branching ratios up to two orders of magnitude larger than the analogue branching ratios of the  $CP$ -even Flavon. For the parameter values used here, the main decay channels of the  $CP$ -odd Flavon would be  $A_F \rightarrow \bar{t}c$ ,  $A_F \rightarrow \bar{b}b$ ,  $A_F \rightarrow \tau\mu$ , whereas the  $A_F \rightarrow \bar{t}t$  decay would be very suppressed due to the  $A_F \bar{t}t$  coupling. The one-loop decays  $A_F \rightarrow \gamma\gamma$  and  $A_F \rightarrow \gamma Z$  would also have very small branching ratios of the order of  $10^{-8}$ .

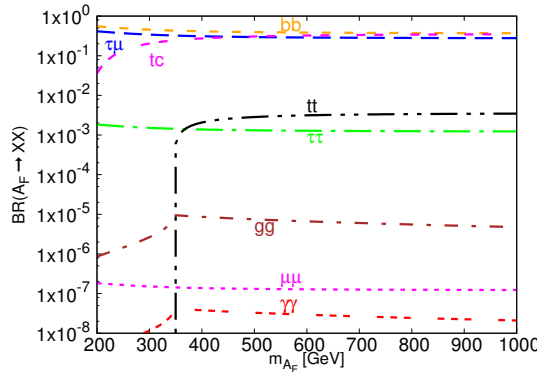


FIG. 7: The same as in Fig. 6 but for the  $CP$ -odd Flavon.

## 2. Three-body decays $H_F \rightarrow \bar{f}_i f_j h$

At the tree-level the  $CP$ -even Flavon also couples with a fermion pair and a SM Higgs boson, thus it is worth analyzing the behavior of the three-body decay modes  $H_F \rightarrow \bar{f}_i f_j h$ . The corresponding decay width is presented in Appendix B. In Fig. 8 we show the branching ratios for these three-body decays. We observe that, for a relatively light Flavon with mass around 300 GeV, the decay channel  $H_F \rightarrow \bar{b}bh$  would have a branching ratio as large as  $10^{-1}$ . On the other hand, other kinematically allowed  $H_F \rightarrow \bar{f}_i f_j h$  decays would reach branching ratios as high as  $10^{-2}$ . For a heavier Flavon with  $m_{H_F} > 600$  GeV, the decay  $H_F \rightarrow \bar{t}th$  would become open and could be the dominant three-body decay mode for  $m_{H_F} \simeq 900$  GeV. Although these decay channels seem worth a more detailed study, we will content ourselves with obtaining the event numbers that could be achieved at the LHC and the FCC. We consider values for the luminosities of the table II. In the Fig. 9 we show the number of events for the processes  $pp \rightarrow H_F \rightarrow q\bar{q}h$  with  $q = b, t$ .

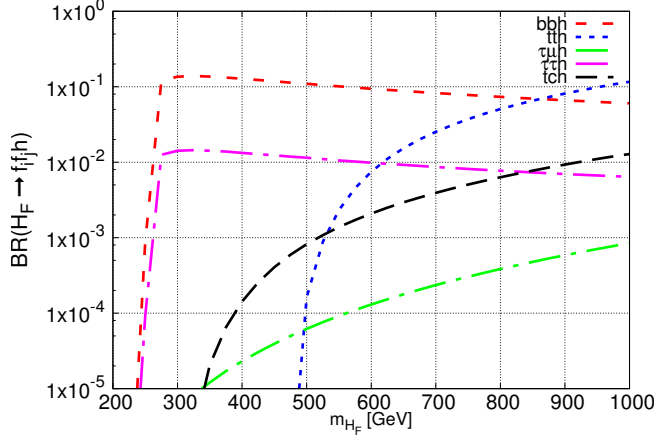


FIG. 8: Branching ratios for the three-body decay modes  $H_F \rightarrow \bar{f}_i f_j h$  as functions of  $m_{H_F}$  for the parameters of Table I.

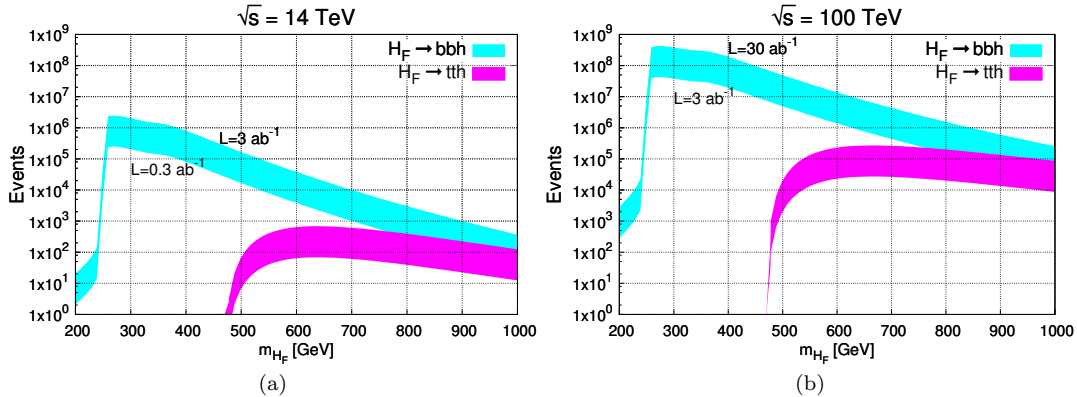


FIG. 9: Event number for the process  $pp \rightarrow H_F \rightarrow q\bar{q}h$  ( $q = b, t$ ) as a function of  $m_{H_F}$ : (a)  $\sqrt{s} = 14$  TeV for an integrated luminosity from  $\mathcal{L}=0.3 \text{ ab}^{-1}$  (lower limit) to  $3 \text{ ab}^{-1}$  (upper limit) and (b)  $\sqrt{s} = 100$  TeV for an integrated luminosity from  $\mathcal{L}=3 \text{ ab}^{-1}$  (lower limit) to  $30 \text{ ab}^{-1}$  (upper limit). The parameters of Table I were used.

## C. Search for LFV Flavon decays at the LHC and a future 100 TeV $pp$ collider

We are interested in the possible detection of the  $CP$ -even and  $CP$ -odd Flavons via their LFV decay into a  $\tau\mu$  pair at the LHC and the FCC. We thus show in Fig. 10 the event numbers for the processes  $pp \rightarrow H_F \rightarrow \tau\mu$  and  $pp \rightarrow A_F \rightarrow \tau\mu$ , for  $\sqrt{s} = 14$  (100) TeV and an integrated luminosity for the values displayed in the Table II. We also use the same set of parameter values of Table I. We note that for a  $CP$ -even Flavon with a mass about 1 TeV,

there would be about  $\mathcal{O}(10)$   $\mu\tau$  signal events at the LHC and  $\mathcal{O}(10^4)$  events at the FCC. These event numbers would decrease by about two orders of magnitude for a  $CP$ -odd Flavon.

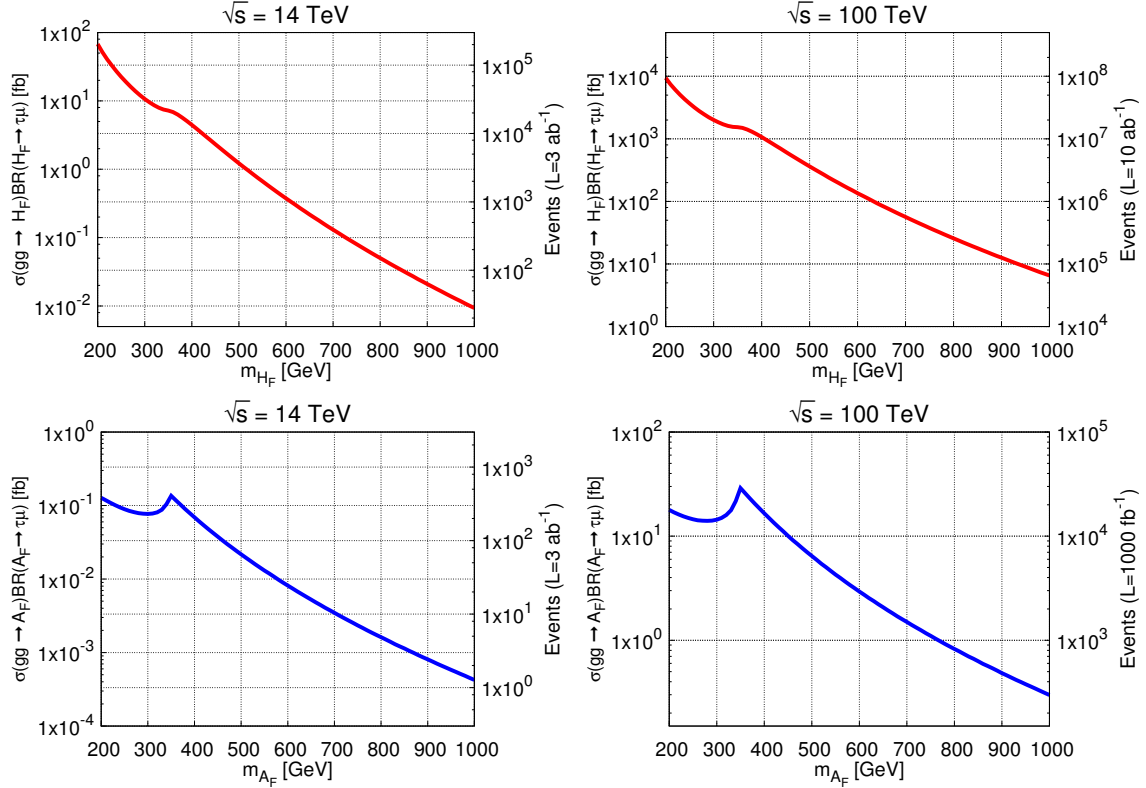


FIG. 10:  $\sigma(pp \rightarrow H_F \rightarrow \tau\mu)$  (top plots) and  $\sigma(pp \rightarrow A_F \rightarrow \tau\mu)$  (bottom plots) cross sections as functions of the Flavon mass for  $\sqrt{s} = 14$  TeV (left plot) and  $100$  TeV (right plots). On the right axes we show the event numbers considering an integrated luminosity  $\mathcal{L}$  of  $3 \text{ ab}^{-1}$  and  $10 \text{ ab}^{-1}$ .

We will now analyze the signature of the LFV Flavon decays  $H_F \rightarrow \tau\mu$  and  $A_F \rightarrow \tau\mu$ , with  $\tau\mu = \tau^-\mu^+ + \tau^+\mu^-$ , and their potential SM background. We are inspired in the analysis carried out by the CMS collaboration in Refs. [23], ATLAS collaboration [39] and the work of the authors of [40]. The ATLAS and CMS collaborations considered the two following tau decay channels: electron decay  $\tau_e\mu$  and the hadron decay  $\tau_h\mu$ . For our analysis we will concentrate instead on the electron decay. As far as our computation scheme is concerned, we first use the LanHEP routines to obtain the FNSM Feynman rules for Madgraph [41]. In this way, the signal and background events can be generated by MadGraph5 and MadGraph5\_aMC@NLO, respectively, interfaced with Pythia 6 [42] and Delphes 3 [43] for detector simulations. The background events were generated at NLO in QCD and the signal at LO, using the CT10 parton distribution functions [44]. The signal and main background events are as follows:

- **Signal:** the signal is  $gg \rightarrow \phi \rightarrow \tau\mu \rightarrow e\nu_e\nu_\tau\mu$  with  $\phi = H_F, A_F$ . The electron channel must contain exactly two opposite-charge leptons, one an electron and the other a muon. Then, we search for the final state  $e\mu + \text{miss energy}$ . We consider the specific case for which an integrated luminosity  $\mathcal{L}$  of  $1 \text{ ab}^{-1}$  for the LHC is considered and in the interval  $1 - 20 \text{ ab}^{-1}$  for the FCC.
- **Background:** the main SM background arises from  $Z$  production via the Drell-Yan process, followed by the decay  $Z \rightarrow \tau\tau$  as well as  $W^+W^-$  and  $ZZ$  pair production and jets. In this work we will only consider the main background to assess how our signal could be searched for.

### 1. Analysis at the LHC

We start by analyzing the possible detection of the  $CP$ -even Flavon at the LHC with  $\sqrt{s}=14$  TeV. For illustrative purpose, we use the following set of values for  $m_{H_F}$ : 200, 250, 300, and 350 GeV. We generated  $10^5$  events for the signal and the SM main background. Afterwards, the kinematic analysis was done via MadAnalysis-5 [45]. The cuts

TABLE III: Kinematic cuts applied to the  $pp \rightarrow H_F \rightarrow \tau\mu \rightarrow e\mu + \text{miss energy signal}$  and the SM background at the LHC with a center-of-mass energy  $\sqrt{s} = 14$  TeV and an integrated luminosity of  $\mathcal{L} = 1 \text{ ab}^{-1}$ . We also show the corresponding event numbers obtained after the kinematic cuts and the signal significance  $S/\sqrt{S+B}$  for  $m_{H_F} = 200$  GeV. The transverse mass is defined as  $M_T^\ell = \sqrt{2P_T^\ell E_T^{\text{miss}}(1 - \cos\Delta\phi_{P_T^\ell - E_T^{\text{miss}}})}$ .

Cut number	Cuts	Signal (S)	Background (B)	$\frac{S}{\sqrt{S+B}}$
	Initial (no cuts)	9190	29320240	1.7
1	$ \eta^e  < 2.3$	6348	9644078	2.04
2	$ \eta^\mu  < 2.1$	5185	7736476	1.86
3	$0.1 < \Delta R(e, \mu)$	5185	7727929	1.87
4	$60 < P_T^\mu$	4856	3602928	2.56
5	$20 < P_T^e$	4562	2031748	3.20
6	$20 < M_{\text{inv}}(e, \mu) < 170$	4450	1781998	3.20
7	$10 < \text{MET} < 100$	3504	1158653	3.33
8	$75 < M_T^e$	2942	973054	3.55
9	$60 < M_T^\mu$	2833	585342	3.7

applied to both the signal and background are shown in Table III, where we also show the event numbers of the signal (S) and background (B) after the kinematic cuts are applied, along with the signal significance  $S/\sqrt{S+B}$  for  $m_{H_F} = 200$  GeV. The effect of the cuts on the signal and background event numbers is best illustrated in Fig. 11, where we show how the efficiencies  $\epsilon_{\text{signal}}$  and  $\epsilon_{\text{background}}$  evolve after each cut is successively applied. One can observe that once the kinematic cuts are applied, the resulting signal efficiency is about 0.31, whereas that for the background is around 0.02. With a luminosity of  $0.3 \text{ ab}^{-1}$ , the signal significance is about  $2\sigma$ . However, if we take into account an integrated luminosity of  $3 \text{ ab}^{-1}$  it increases up to  $\sim 6.5\sigma$ . The net effect is shown in Fig. 12, where the signal significance is plotted as a function of the luminosity for the chosen values of  $m_{H_F}$ .

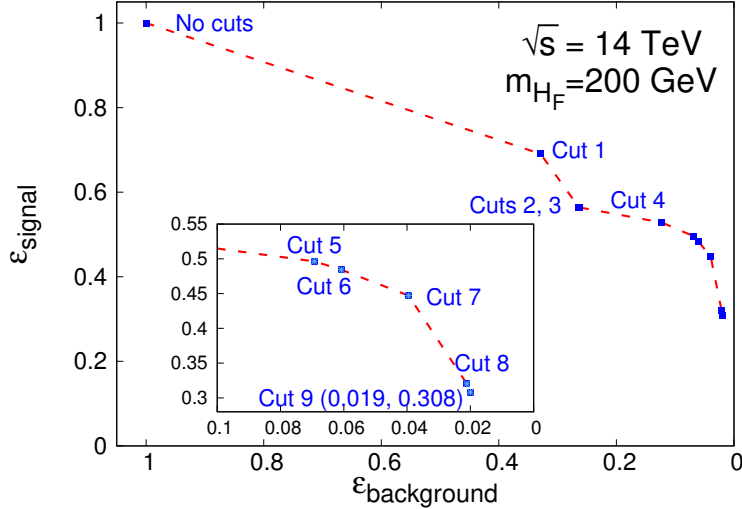


FIG. 11: Evolution of the efficiencies of the  $pp \rightarrow H_F \rightarrow \tau\mu$  signal and the SM background after the kinematic cuts of Table III are successively applied. We use  $m_{H_F} = 200$  GeV and the parameters of Table I.

Therefore, it seems troublesome that a  $CP$ -even Flavon with a mass greater than 300 GeV could be detected at the LHC via the  $H_F \rightarrow \tau\mu$  decay channel. In such a case, we can turn to the decay modes  $H_F \rightarrow WW$  and  $H_F \rightarrow ZZ$ , which are the dominant ones. These decay channels seem more promising for the detection of a heavy Flavon. Along this line, to assess the potentiality of the  $WW$  and  $ZZ$  decay channels for the Flavon detection, we show in Fig. 13 the corresponding event numbers that could be produced at the LHC and a 100 TeV  $pp$  collider. We note that about  $10^5$   $WW$  events would be produced at the LHC for  $m_{H_F} = 1$  TeV, whereas the number of  $ZZ$  events would be slightly smaller. This seems more promising for the signal detection, though a more detailed analysis of the background would be required to draw a definitive conclusion.

As for the  $CP$ -odd Flavon, we notice that it has a smaller  $pp \rightarrow A_F \rightarrow \tau\mu$  production rate, therefore, in order to have evidence of the  $A_F \rightarrow \tau\mu$  decay, higher luminosities, of the order of  $10 \text{ ab}^{-1}$ , would be required. This seems

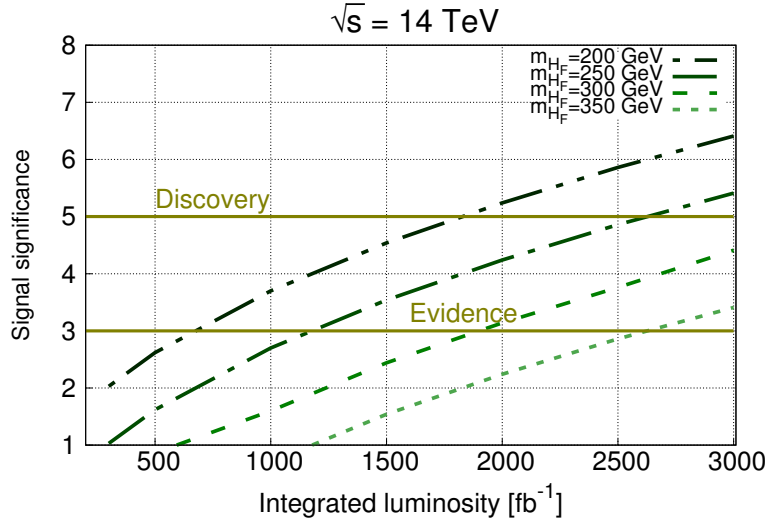


FIG. 12: Signal significance  $S/\sqrt{S+B}$  as a function of the integrated luminosity for the LFV Flavon  $\tau\mu$  decay at the LHC. The horizontal lines show the discovery and evidence thresholds.

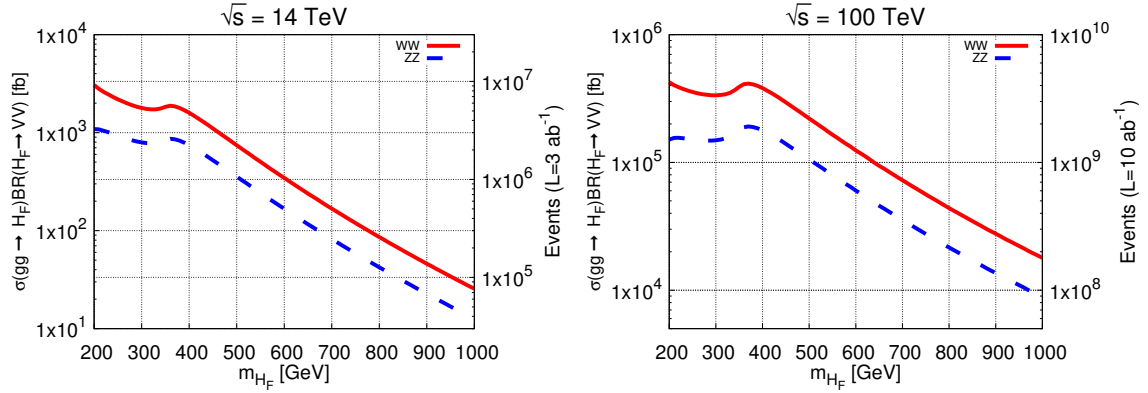


FIG. 13:  $pp \rightarrow H_F \rightarrow WW$  and  $pp \rightarrow H_F \rightarrow ZZ$  event numbers as functions of the Flavon mass at the LHC (left plot) and the FCC (right plot).

inaccessible for the LHC, however, we expect that the search for this decay could be possible at the FCC.

## 2. Analysis at the future 100 TeV pp collider

The building of a 100 TeV  $pp$  collider is under consideration [46]. The luminosity and center-of-mass energy are crucial factors to allow detectable LFV signatures of the FNSM. Luminosity goals for a 100 TeV  $pp$  collider are discussed by the authors of Ref. [46]. Again, we consider the values of the Table II, although up to  $30 \text{ ab}^{-1}$  might be reached. In our analysis we consider the conservative kinematic cuts in order to give a general overview assess how our signal could be searched for. The applied cuts to both the signal and background are shown in Table IV, whereas in Fig. 14 we show the signal significance as a function of the luminosity and the Flavon mass  $m_\phi$ , with  $\phi = H_F, A_F$ . We observe that at a 100 TeV  $pp$  collider with integrated luminosity of  $10 \text{ ab}^{-1}$ , it would be possible to probe  $CP$ -even Flavon masses in the multi-TeV range, up to about 4 TeV. We also notice that  $CP$ -odd Flavon masses could be searched until the order  $\sim 1 \text{ TeV}$ .

TABLE IV: Kinematic cuts applied to the  $pp \rightarrow H_F \rightarrow \tau\mu$  signal and the SM main background at a 100 TeV  $pp$  collider with an integrated luminosity of  $\mathcal{L} = 10 \text{ ab}^{-1}$ . We use the parameter values of Table I and consider a  $CP$ -even Flavon with a mass  $m_{H_F} = 1000 \text{ GeV}$ . We also show the corresponding event numbers obtained after the kinematic cuts, and the signal significance  $S/\sqrt{S+B}$ .

Cut number	Cuts	Signal (S)	Background (B)	$\frac{S}{\sqrt{S+B}}$
	Initial (no cuts)	90720	364075164	4.75
1	$ \eta^e  < 2.3$	80574	310571620	4.57
2	$ \eta^\mu  < 2.1$	73587	262283714	4.54
3	$150 < M_T^e$	45334	117527474	4.18
4	$80 < M_T^\mu$	43765	65354838	5.41
5	$100 < P_T^e$	34252	57819738	4.5
6	$220 < P_T^\mu$	30204	40582493	4.74
7	$100 < MET < 200$	28136	32475178	4.94

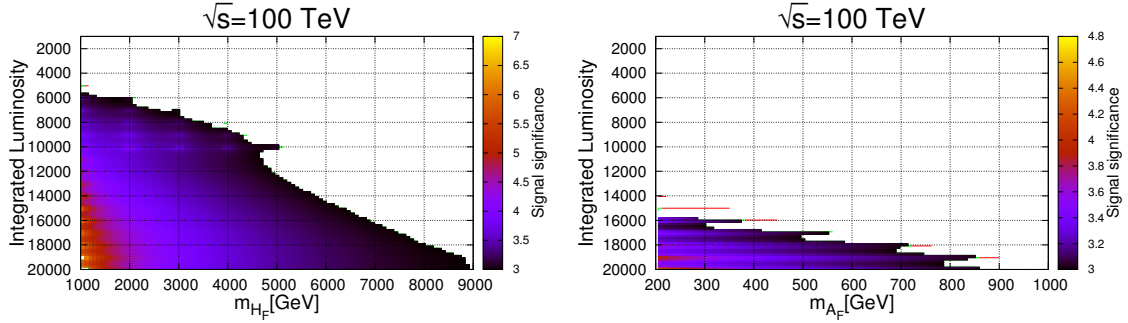


FIG. 14: Density plot for the signal significance as a function of the luminosity and the flavon masses  $m_{H_F}$  and  $m_{A_F}$ .

## V. CONCLUSIONS

In this work we have explored the possibility that the LFV  $\tau\mu$  decay channel of  $CP$ -even  $H_F$  and  $CP$ -odd  $A_F$  Higgs Flavons with a mass of a few hundreds of GeVs could be at the reach of detection at the LHC and a future 100 TeV  $pp$  collider, which would serve as a possible probe of low-scale flavor models. For the theoretical framework, we have considered the simplest Froggatt-Nielsen model, with an Abelian flavor symmetry and a  $CP$ -conserving Higgs sector that includes a Higgs doublet and a Froggatt-Nielsen complex singlet. In this model the  $CP$ -even Flavon can mix with the SM-like Higgs boson, thereby inducing tree-level LFV interactions mediated by the latter. In this work we concentrate instead on the LFV couplings of both the  $CP$ -even and  $CP$ -odd Higgs Flavons. After studying the constraints on the parameter space of the model from low-energy LFV processes, we choose a set of benchmarks and estimate the relevant decay modes and the production cross section of the Flavons via gluon fusion at the LHC and a future 100 TeV  $pp$  collider. We then consider a set of kinematic cuts for both the signal and the SM main background. It is found that the LHC has the potential to discover the LFV decay  $H_F \rightarrow \tau\mu$  for  $m_{H_F}$  between 200 and 350 GeVs provided that luminosities, of the order of  $1-3 \text{ ab}^{-1}$ , are achieved. In such a case other decay channels would be more appropriate to search for the signal of a Flavon at the LHC. As far as a future 100 TeV  $pp$  collider is concerned, it would be able to probe the LFV  $\tau\mu$  decay channel for Flavon masses as heavy as 10 TeVs, as long as an integrated luminosity of at least  $20 \text{ ab}^{-1}$  was available, which has been deemed viable in the literature regarding the possible construction of such a collider. Therefore, besides other physics goals, a 100 TeV Collider might also work as a Flavon factory.

## Acknowledgments

We acknowledge support from Conacyt and SNI (México). Partial support from VIEP-BUAP is also acknowledged.

### Appendix A: Flavon contributions to LFV $h$ and $\tau$ decays and the muon anomaly

In this Appendix we present the analytical expressions necessary to obtain the constraints on the LFV Flavons couplings shown in Fig. 2. Although these results were meant for  $CP$ -even and  $CP$ -odd scalar bosons, they are also valid for the Flavons.

In the FNSM, the LFV decay  $h \rightarrow \tau\mu$  proceeds at the tree-level. The decay width can be obtained from Eq. (B1) of Appendix B in the  $m_h \gg m_\tau \gg m_\mu$  limit. The result is given by

$$\Gamma(h \rightarrow \tau\mu) = \frac{g_{h\mu\tau} m_h}{8\pi}. \quad (\text{A1})$$

The CMS collaboration reported a bound on the respective branching ratio:  $BR(h \rightarrow \bar{\mu}\tau) < 1.2 \times 10^{-2}$  [24].

As far as the  $\tau \rightarrow \mu\gamma$  decay is concerned, it arises at the one-loop level and receives contributions of the SM Higgs boson and the Flavons via the Feynman diagram of Fig. 15(a). The respective decay width is

$$\Gamma(\tau \rightarrow \mu\gamma) = \frac{\alpha m_\tau^5}{64\pi^4} (|C_S|^2 + |C_P|^2), \quad (\text{A2})$$

where the  $C_S$  and  $C_P$  coefficients stand for the contribution of  $CP$ -even and  $CP$ -odd scalar bosons, respectively, which in the limit of  $g_{\phi\tau\tau} \gg g_{\phi\mu\mu} \gg g_{\phi ee}$  ( $\phi = h, H_F, A_F$ ) and  $m_\tau \gg m_\mu \gg m_e$ , can be approximated as [47]

$$C_S = C_P \simeq \sum_{\phi=h, H_F, A_F} \frac{g_{\phi\tau\tau} g_{\phi\mu\tau}}{12m_\phi^2} \left( 3 \ln \left( \frac{m_\phi^2}{m_\tau^2} \right) - 4 \right). \quad (\text{A3})$$

Two-loop contributions can be relevant and the respective expressions are reported in [47]. The current experimental limit on the branching ratio is  $BR(\tau \rightarrow \mu\gamma) < 4.4 \times 10^{-8}$  [34].

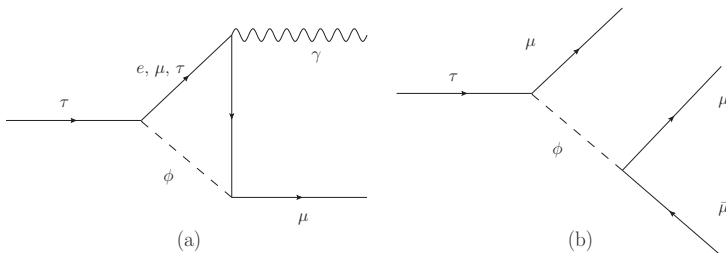


FIG. 15: Feynman diagrams for the LFV decays  $\tau \rightarrow \mu\gamma$  and  $\tau \rightarrow \mu\bar{\mu}\mu$  with exchange of a scalar boson  $\phi$ . We omit both the bubble diagrams for the decay  $\tau \rightarrow \mu\gamma$ , which only serve to cancel the ultraviolet divergences, and the diagram where there is the exchange of the final muons in diagram (b).

As for the  $\tau \rightarrow \mu\bar{\mu}\mu$  decay, it receives contributions from the exchange of a SM-Higgs boson and the Flavons as depicted in the Feynman diagram of Fig. 15(b). The tree-level decay width can be approximated as

$$\Gamma(\tau \rightarrow \mu\bar{\mu}\mu) \simeq \frac{m_\tau^5}{256\pi^3} \left( \frac{S_h^2}{m_h^4} + \frac{S_{H_F}^2}{m_{H_F}^4} + \frac{S_{A_F}^2}{m_{A_F}^4} + \frac{2S_h S_{H_F}}{m_h^2 m_{H_F}^2} + \frac{2S_{A_F}}{3m_{A_F}^2} \left( \frac{S_h}{m_h^2} + \frac{S_{H_F}}{m_{H_F}^2} \right) \right), \quad (\text{A4})$$

where  $S_\phi = g_{\phi\mu\mu} g_{\phi\mu\tau}$ . It has been pointed in Ref. [47], however, that the one-loop contribution is dominant. We refrain from presenting the corresponding expression as this process, for which the experimental limit on the respective branching ratio is  $BR(\tau \rightarrow \mu\bar{\mu}\mu) < 2.1 \times 10^{-8}$  [34], gives very weak constraints on the FNSM parameters.

Finally, the muon AMDM also receives contributions from the SM Higgs boson and the Flavons, which are induced by a triangle diagram similar to the diagram of Fig. 15(a) but with two external muons. The corresponding contribution can be approximated for  $m_\phi \gg m_l$  as [47]

$$\delta a_\mu \sim \frac{m_\mu}{16\pi^2} \sum_{\phi=h, H_F, A_F} \sum_{l=\mu, \tau} \frac{m_l g_{\phi\mu l}^2}{m_\phi^2} \left( 2 \ln \left( \frac{m_\phi^2}{m_l^2} \right) - 3 \right), \quad (\text{A5})$$

where one must take into account the NP corrections to the  $g_{h\mu\mu}$  coupling only. If the Flavons are too heavy, the dominant NP contribution would arise from the SM Higgs boson.

The discrepancy between SM theoretical prediction and the experimental value is [34]

$$\Delta a_\mu = a_\mu^{exp} - a_\mu^{SM} = (2.88 \pm 0.63 \pm 0.49) \times 10^{-9}. \quad (\text{A6})$$

Thus, the requirement that this discrepancy is accounted for by Eq. (A5) leads to the bound  $1.32 \times 10^{-9} \leq \Delta a_\mu \leq 4.44 \times 10^{-9}$  with 95% C.L.

## Appendix B: Decay widths of $CP$ -even and $CP$ -odd scalar bosons

### 1. $CP$ -even scalar boson decays

The most relevant decays of both  $CP$ -even and  $CP$ -odd scalar bosons  $\phi$  have been long studied in the literature. We will present the relevant decay widths for the sake of completeness as they are also valid for the Flavons. We will assume that all the couplings are SM-like, other than the  $g_{HP_1P_2}$  couplings, which stand for the couplings of a  $CP$ -odd scalar boson  $H$  with the  $P_1$  and  $P_2$  particles. The tree-level two-body widths are as follows.

The  $\phi \rightarrow \bar{f}_i f_j$  decay width is given by

$$\Gamma(\phi \rightarrow \bar{f}_i f_j) = \frac{g_{\phi f_i f_j}^2 N_c m_\phi}{128\pi} (4 - (\sqrt{\tau_{f_i}} + \sqrt{\tau_{f_j}})^2)^{\frac{3}{2}} \sqrt{4 - (\sqrt{\tau_{f_i}} - \sqrt{\tau_{f_j}})^2}, \quad (\text{B1})$$

where  $\tau_i = 4m_i^2/m_\phi^2$  and  $N_c$  is the color number. From here we easily obtain the flavor conserving decay width.

The decays of a heavy  $CP$ -even scalar boson into pairs of real electroweak gauge bosons can also be kinematically allowed. The corresponding decay width is

$$\Gamma(\phi \rightarrow VV) = \frac{g_{HVV}^2 m_\phi^3}{64n_V \pi m_V^4} \sqrt{1 - \tau_V} \left( 1 - \tau_V + \frac{3}{4} \tau_V^2 \right), \quad (\text{B2})$$

with  $n_V = 1$  (2) for  $V = W$  ( $Z$ ).

Other relevant decays are those arising at the one-loop level, such as  $\phi \rightarrow \gamma\gamma$  and  $\phi \rightarrow gg$ . The two-photon decay width can be written as

$$\Gamma(\phi \rightarrow \gamma\gamma) = \frac{\alpha^2 m_\phi^3}{1024\pi^3 m_W^2} \left| \sum_s A_s^{\phi\gamma\gamma}(\tau_s) \right|^2, \quad (\text{B3})$$

with the subscript  $s$  standing for the spin of the charged particle circulating into the loop. The  $A_s^{\phi\gamma\gamma}$  function is given by

$$A_s^{\phi\gamma\gamma}(\tau_s) = \begin{cases} \sum_f \frac{2m_W g_{\phi f} N_c Q_f^2}{m_f} [-2\tau_s (1 + (1 - \tau_s)f(\tau_s))] & s = \frac{1}{2}, \\ \frac{g_{\phi WW}}{m_W} [2 + 3\tau_W + 3\tau_W(2 - \tau_W)f(\tau_W)] & s = 1, \\ \frac{m_W g_{\phi H^- H^+}}{m_S^2} [\tau_{\phi^\pm} (1 - \tau_{\phi^\pm} f(\tau_{\phi^\pm}))] & s = 0, \end{cases} \quad (\text{B4})$$

where

$$f(x) = \begin{cases} \left[ \arcsin \left( \frac{1}{\sqrt{x}} \right) \right]^2 & x \geq 1, \\ -\frac{1}{4} \left[ \log \left( \frac{1+\sqrt{1-x}}{1-\sqrt{1-x}} \right) - i\pi \right]^2 & x < 1. \end{cases} \quad (\text{B5})$$

On the other hand, the two-gluon decay can receive contributions of quarks only and the respective decay width can be obtained from Eq. (B3) by summing over quarks only and making the replacements  $\alpha^2 \rightarrow 2\alpha_S^2$ ,  $N_c Q_f^2 \rightarrow 1$ .

Formulas for other decay channels such as  $\phi \rightarrow Z\gamma$ , which has a considerably suppressed decay width, as well as radiative corrections for the above decay widths can be found in the literature [48, 49].

## 2. $CP$ -odd scalar boson decays

The decay of a  $CP$ -odd scalar boson  $A$  into a pair of fermions of distinct flavor is given by

$$\Gamma(A \rightarrow \bar{f}_i f_j) = \frac{g_{A f_i f_j}^2 N_c m_A}{128\pi} (4 - (\sqrt{\eta_{f_i}} - \sqrt{\eta_{f_j}})^2)^{\frac{3}{2}} \sqrt{4 - (\sqrt{\eta_i} + \sqrt{\eta_j})^2}, \quad (\text{B6})$$

where we now use the definition  $\eta_i = 4m_i^2/m_A^2$ . The FC decay width follows easily.

There are no decays into electroweak gauge bosons at the tree-level. On the other hand, the two-photon decay proceeds through charged fermion loops only and the corresponding decay width can be obtained from (B3) by making the replacement  $\phi \rightarrow A$  and summing over fermions only, with

$$A_{1/2}^{A\gamma\gamma}(\tau_f) = \sum_f \frac{2m_W g_{A\bar{f}f} Q_f^2 N_c}{m_f} (-2\tau_f f(\tau_f)), \quad (\text{B7})$$

whereas the two-gluon decay width can be obtained by summing over quarks only and making the additional replacements  $\alpha^2 \rightarrow 2\alpha_S^2$  and  $N_c Q_f^2 \rightarrow 1$ .

## 3. Three-body decay $H_F \rightarrow \bar{f}f h$

As far as three-body decays are concerned, the study of the  $H \rightarrow \bar{f}f h$  decay channel could be interesting as it can also have a sizeable branching ratio. This decay receives contribution from the four Feynman diagrams shown in Fig. 16. After some algebra, we can write the decay width as follows

$$\Gamma(H_F \rightarrow h\bar{f}f) = \frac{m_{H_F}}{256\pi^3} \int dx_a \int dx_b |\bar{\mathcal{M}}(H_F \rightarrow h\bar{f}f)|^2, \quad (\text{B8})$$

where the integration domain is given by

$$2\sqrt{x_t} \leq x_a \leq 1 - x_h - 2\sqrt{x_t x_h}, \quad (\text{B9})$$

$$x_b \gtrless \frac{2(1 - x_h + 2x_t) + x_a(x_a + x_h - 2x_t - 3) \mp \sqrt{x_a^2 - 4x_t} \sqrt{(x_a + x_h - 1)^2 - 4x_h x_t}}{2(1 - x_a + x_t)} \quad (\text{B10})$$

and the average square amplitude is

$$\begin{aligned} |\bar{\mathcal{M}}(H_F \rightarrow h\bar{f}f)|^2 = & \frac{1}{2(x_a + x_b + x_h - 2)^2} (x_a + x_b + x_h - 4x_t - 1) ((x_a + x_b + x_h - 2) C_a + C_b)^2 \\ & + \frac{2}{(x_a - 1)^2 (x_b - 1)^2} \left( (x_a - 1)(x_b - 1)(x_a - x_b)^2 - 16(x_a + x_b - 2)^2 x_t^2 \right. \\ & + 4(x_a + x_b - 2)(2 - 3x_b + x_a(4x_b - 3))x_t + x_h \left( 4(x_a + x_b - 2)^2 x_t - (x_a - x_b)^2 \right) \left. C_c^2 \right. \\ & - \frac{4\sqrt{x_t}}{(x_a - 1)(x_b - 1)} (x_a^2 + 2(3x_b + x_h - 4x_t - 3)x_a + x_b^2 - 4x_h + 2x_b(x_h - 4x_t - 3) + 16x_t + 4) C_a C_c \\ & - \frac{4\sqrt{x_t}}{(x_a - 1)(x_b - 1)(x_a + x_b + x_h - 2)} \left( x_a^2 + 2(3x_b + x_h - 4x_t - 3)x_a + x_b^2 - 4x_h \right. \\ & \left. + 2x_b(x_h - 4x_t - 3) + 16x_t + 4 \right) C_b C_c. \end{aligned} \quad (\text{B11})$$

with  $x_a = (m_a/m_{H_F})^2$ . Also  $C_a = g_{H_F f f h}$ ,  $C_b = g_{H_F h h} g_{h f f}/m_h^2$ , and  $C_c = g_{H_F f f} g_{h f f}/m_h$  are the coupling constants involved in the Feynman diagrams of Fig. 16.

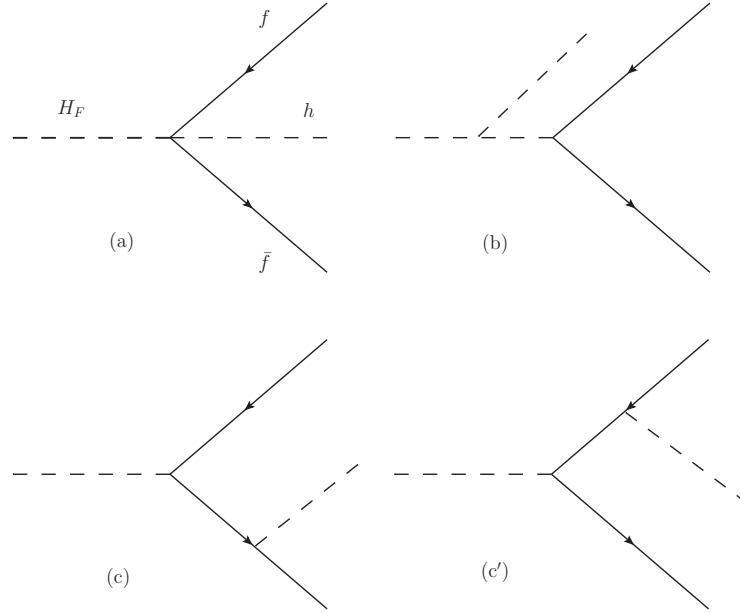


FIG. 16: Feynman diagrams inducing the  $H \rightarrow \bar{f}f h$  decay in the FNSM.

The general expressions for the FV decay  $H_F \rightarrow f_i f_j h$  are to cumbersome unless one of the masses is neglected, so we refrain from presenting it here. The calculation was done instead via the CalcHEP software.

---

[1] G. Aad et al. (ATLAS), Phys. Lett. **B716**, 1 (2012), 1207.7214.  
[2] S. Chatrchyan et al. (CMS), Phys. Lett. **B716**, 30 (2012), 1207.7235.  
[3] J. F. Gunion, H. E. Haber, G. L. Kane, and S. Dawson, Front. Phys. **80**, 1 (2000).  
[4] A. Pomarol, in *Proceedings, High-energy Physics. Proceedings, 18th European School (ESHEP 2010): Raseborg, Finland, June 20 - July 3, 2010* (2012), pp. 115–151, 1202.1391, URL <https://inspirehep.net/record/1088246/files/arXiv:1202.1391.pdf>.  
[5] S. P. Martin (1997), [Adv. Ser. Direct. High Energy Phys.18,1(1998)], hep-ph/9709356.  
[6] J. R. Espinosa, C. Grojean, M. Muhlleitner, and M. Trott, JHEP **05**, 097 (2012), 1202.3697.  
[7] P. P. Giardino, K. Kannike, I. Masina, M. Raidal, and A. Strumia, JHEP **05**, 046 (2014), 1303.3570.  
[8] G. C. Branco, P. M. Ferreira, L. Lavoura, M. N. Rebelo, M. Sher, and J. P. Silva, Phys. Rept. **516**, 1 (2012), 1106.0034.  
[9] J. L. Diaz-Cruz, R. Noriega-Papaqui, and A. Rosado, Phys. Rev. **D69**, 095002 (2004), hep-ph/0401194.  
[10] J. L. Diaz-Cruz, R. Noriega-Papaqui, and A. Rosado, Phys. Rev. **D71**, 015014 (2005), hep-ph/0410391.  
[11] J. L. Diaz-Cruz, JHEP **05**, 036 (2003), hep-ph/0207030.  
[12] E. Ma (2009), 0905.0221.  
[13] A. Pilaftsis, Phys. Lett. **B285**, 68 (1992).  
[14] J. L. Diaz-Cruz and J. J. Toscano, Phys. Rev. **D62**, 116005 (2000), hep-ph/9910233.  
[15] T. Han and D. Marfatia, Phys. Rev. Lett. **86**, 1442 (2001), hep-ph/0008141.  
[16] K. A. Assamagan, A. Deandrea, and P.-A. Delsart, Phys. Rev. **D67**, 035001 (2003), hep-ph/0207302.  
[17] E. Arganda, A. M. Curiel, M. J. Herrero, and D. Temes, Phys. Rev. **D71**, 035011 (2005), hep-ph/0407302.  
[18] A. Brignole and A. Rossi, Nucl. Phys. **B701**, 3 (2004), hep-ph/0404211.  
[19] J. L. Diaz-Cruz, D. K. Ghosh, and S. Moretti, Phys. Lett. **B679**, 376 (2009), 0809.5158.  
[20] S. Chamorro-Solano, A. Moyotl, and M. A. Pérez (2017), 1707.00100.  
[21] S. Chamorro-Solano, A. Moyotl, and M. A. Pérez, J. Phys. Conf. Ser. **761**, 012051 (2016).  
[22] A. Lami and P. Roig, Phys. Rev. **D94**, 056001 (2016), 1603.09663.  
[23] V. Khachatryan et al. (CMS), Phys. Lett. **B749**, 337 (2015), 1502.07400.  
[24] C. Collaboration (CMS) (2016).  
[25] G. Isidori, Y. Nir, and G. Perez, Ann. Rev. Nucl. Part. Sci. **60**, 355 (2010), 1002.0900.  
[26] A. Bolaños, J. L. Diaz-Cruz, G. Hernández-Tomé, and G. Tavares-Velasco, Phys. Lett. **B761**, 310 (2016), 1604.04822.  
[27] M. Bauer, T. Schell, and T. Plehn, Phys. Rev. **D94**, 056003 (2016), 1603.06950.  
[28] K. Huitu, V. Keus, N. Koivunen, and O. Lebedev, JHEP **05**, 026 (2016), 1603.06614.  
[29] E. L. Berger, S. B. Giddings, H. Wang, and H. Zhang, Phys. Rev. **D90**, 076004 (2014), 1406.6054.

- [30] J. L. Diaz-Cruz and U. J. Saldaña-Salazar, Nucl. Phys. **B913**, 942 (2016), 1405.0990.
- [31] R. Contino et al., CERN Yellow Report pp. 255–440 (2017), 1606.09408.
- [32] T. Golling et al., CERN Yellow Report pp. 441–634 (2017), 1606.00947.
- [33] C. Bonilla, D. Sokolowska, N. Darvishi, J. L. Diaz-Cruz, and M. Krawczyk, J. Phys. **G43**, 065001 (2016), 1412.8730.
- [34] C. Patrignani et al. (Particle Data Group), Chin. Phys. **C40**, 100001 (2016).
- [35] G. Aad et al. (ATLAS), JHEP **11**, 211 (2015), 1508.03372.
- [36] M. A. Arroyo-Ureña, J. L. Diaz-Cruz, E. Díaz, and J. A. Orduz-Ducuara, Chin. Phys. **C40**, 123103 (2016), 1306.2343.
- [37] A. Belyaev, N. D. Christensen, and A. Pukhov, Comput. Phys. Commun. **184**, 1729 (2013), 1207.6082.
- [38] A. Semenov, Comput. Phys. Commun. **201**, 167 (2016), 1412.5016.
- [39] G. Aad et al. (ATLAS), Eur. Phys. J. **C77**, 70 (2017), 1604.07730.
- [40] R. Primulando and P. Uttayarat, JHEP **05**, 055 (2017), 1612.01644.
- [41] J. Alwall, M. Herquet, F. Maltoni, O. Mattelaer, and T. Stelzer, JHEP **06**, 128 (2011), 1106.0522.
- [42] T. Sjostrand, S. Mrenna, and P. Z. Skands, JHEP **05**, 026 (2006), hep-ph/0603175.
- [43] J. de Favereau, C. Delaere, P. Demin, A. Giammanco, V. Lemaître, A. Mertens, and M. Selvaggi (DELPHES 3), JHEP **02**, 057 (2014), 1307.6346.
- [44] J. Gao, M. Guzzi, J. Huston, H.-L. Lai, Z. Li, P. Nadolsky, J. Pumplin, D. Stump, and C. P. Yuan, Phys. Rev. **D89**, 033009 (2014), 1302.6246.
- [45] E. Conte, B. Fuks, and G. Serret, Comput. Phys. Commun. **184**, 222 (2013), 1206.1599.
- [46] N. Arkani-Hamed, T. Han, M. Mangano, and L.-T. Wang, Phys. Rept. **652**, 1 (2016), 1511.06495.
- [47] R. Harnik, J. Kopp, and J. Zupan, JHEP **03**, 026 (2013), 1209.1397.
- [48] A. Djouadi, Phys. Rept. **457**, 1 (2008), hep-ph/0503172.
- [49] A. Djouadi, Phys. Rept. **459**, 1 (2008), hep-ph/0503173.